Journal of Industrial and Engineering Chemistry 138 (2024) 153–164

Contents lists available at ScienceDirect

Journal of Industrial and Engineering Chemistry

journal homepage: www.elsevier.com/locate/jiec

Waste-derived tuff for CO_2 Capture: Enhanced CO_2 adsorption performances by Cation-Exchange tailoring

F. Raganati [a], F. Miccio [b], G. Iervolino [c], E. Papa [b], P. Ammendola [a,*]

[a] Istituto di Science e Tecnologie per l'Energia e la Mobilità Sostenibili (STEMS) - CNR, Piazzale V. Tecchio 80, 80125 Naples, Italy
[b] Istituto di Scienza e Tecnologia dei Materiali Ceramici (ISTEC) - CNR, via Granarolo, 64, 48018 Faenza, RA, Italy
[c] Department of Industrial Engineering, University of Salerno, via Giovanni Paolo II, 132, 84084 Fisciano, SA, Italy

ARTICLE INFO

Keywords:
Waste-derived Tuff
Natural Zeolites
Cation-exchange
Fixed-bed adsorption
Thermodynamics
Freundlich isotherms

ABSTRACT

Mitigating greenhouse gas emissions through CO_2 capture from industrial flue gases is imperative for addressing climate change. This article delves into the potential of natural tuff, derived from construction and demolition (C&D) waste, as an affordable and sustainable CO_2 adsorbent for post-combustion capture. By tailoring the tuff structure and chemical composition through cation-exchange, the crucial role of cation type in enhancing its textural properties, particularly its microporosity and specific surface area, has been highlighted. Notably, Li- and Na-exchanges greatly enhance these properties, indicating a heightened potential for CO_2 capture. The work further explores the dynamic CO_2 adsorption of both untreated and modified tuff in a fixed-bed reactor under low CO_2 partial pressures (< 0.2 atm), particularly examining the effects of extra-framework cation nature (Na^+, Li^+) and composition, and the influence of NH_4^+ pre-treatment. Results show that Na- and Li-exchanged tuff exhibit enhanced CO_2 uptake (up to 1 mmol g^{-1}) compared to untreated tuff (0.54 mmol g^{-1}), with Li-exchange resulting in the highest capacity due to both superior textural properties and stronger ion-quadrupole interactions with CO_2 molecules. The multi-cyclic stability of the synthesized samples has been also assessed; regardless of the specific cation-exchange type, all the samples provide stable performances over 10 consecutive adsorption/desorption cycles.

Introduction

Out of the various strategies for separating CO_2, such as pre-combustion capture, post-combustion capture, and oxy-fuel combustion [1], post-combustion capture is considered to be a feasible option for fossil fuel-fired plants in the short term [2]. This involves selectively removing CO_2 from gaseous effluent, without needing major modifications to existing facilities and processes [3]. Although amine-based or ammonia-based absorption methods are the most mature technologies for CO_2 separation, they have several disadvantages when applied to post-combustion applications. These include the need for significant amounts of energy to regenerate the sorbent, corrosion problems, degradation of the amines due to exposure to oxygen, and loss of amines through evaporation, which can result in environmental consequences [4].

Adsorption using solid sorbents has gained considerable attention as a viable option in the Carbon Capture and Storage (CCS) framework due to its several advantages, such as low regeneration energy consumption, high selectivity, ease of handling, absence of liquid waste streams, and a broad range of operability at different temperatures [5]. Typically, adsorption is performed in two fixed-bed reactors. The feed stream containing the adsorbate is passed through the first bed. Once the adsorbate concentration reaches a specific threshold value, the reactor is taken off-line and the feed is directed towards the second bed to avoid breakthrough. Meanwhile, the first bed undergoes regeneration, which can be achieved through either an increase in temperature (temperature swing adsorption, TSA) or a decrease in pressure (pressure swing adsorption, PSA) [6,7]. For this approach to succeed, the sorbent should be versatile, exhibit excellent performance at low CO_2 pressure (a typical range for the CO_2 pressure in post-combustion conditions is up to 0.2 atm [3]), possess a high capacity for CO_2 adsorption, fast kinetics for both adsorption and desorption processes, high selectivity for CO_2, the ability to withstand mild regeneration conditions, robustness in terms of its ability to endure repetitive adsorption and desorption cycles, tolerance towards moisture and other impurities present in the feed, as well as sufficient mechanical strength [5]. With reference to the tolerance

* Corresponding author.
E-mail address: paola.ammendola@stems.cnr.it (P. Ammendola).

https://doi.org/10.1016/j.jiec.2024.03.049
Received 26 December 2023; Received in revised form 6 March 2024; Accepted 27 March 2024
Available online 30 March 2024

towards moisture in the feed, it is well known that its presence causes the reduction in the adsorption capacity of most of the currently well-developed CO_2 adsorbents (such as activated carbons and zeolites) [8]. Therefore, the limiting step is the development of sorbents with specific properties, for which adsorption of water and other impurities would not be competitive with that of CO_2, to avoid the need of an upstream drying/purification step, which would adversely impact the CO_2 capture economics [8].

Sorbents can be categorized into either physical or chemical sorbents (physisorbents and chemisorbents) based on the mechanism of sorption [9]. Physisorption is a process where the interaction between the adsorbate and adsorbent is relatively weak, usually involving van der Waals forces. Chemisorption, on the other hand, involves stronger chemical interactions between the adsorbate and adsorbent, resulting in the transfer of electrons [9]. Materials such as porous carbonaceous materials [5,10–17], zeolites [18,19], alumina [20], silica gels [21], and geopolymers [22,23] are commonly used as physisorbents. These materials are chosen for their diverse properties, such as high surface area, tunable porosity, and chemical stability, which make them effective for physisorption-based applications. Porous carbonaceous materials, for instance, offer a wide range of structures and functionalities [24–27], while zeolites provide well-defined porous frameworks [18,19]. Polymers, on the other hand, are recognized as having the ability to to achieve tunable porosity, undergo synthetic diversification, and maintain excellent physicochemical stability [28]. On the contrary, chemisorbents, like sorbents functionalized with amines, typically contain basic sites, such as carbonates and amino groups, which can form strong interactions with the acidic CO_2 molecules [29,30]. Additionally, some sorbents like metal organic frameworks (MOFs) can offer both physical and chemical interactions with CO_2 [18,28,31]. Physical adsorption of CO_2 is a promising option in this context because the process is completely reversible, which means that the sorbent can be regenerated with relatively low energy requirements due to the lower adsorption enthalpy compared to chemical sorbents [3].

Synthetic zeolites are highly ordered microporous crystalline materials that are synthesized with a precise and appropriate molecular cell, pore size, and type of extra-framework cations, all of which specifically affect their adsorption performance [32]. However, synthetic zeolites have limitations in terms of sustainability due to their high synthesis cost and environmental impact [22,33]. A potential solution to this problem is the use of natural zeolites, which are abundant in various regions worldwide and occur naturally in different types of rocks [34,35]. Despite their advantages of abundance and low cost, natural zeolites have drawbacks such as variable composition, low purity, and potentially lower separation performance compared to synthetic zeolites [34]. Volcanic tuffs, containing various minerals such as clinoptilolite, mordenite, chabazite, quartz, cristobalite, and feldspar [36], are the most valuable deposits of natural zeolites [37]. Besides, tuff is often found in construction and demolition (C&D) waste, namely solid waste materials generated from construction, demolition, and renovation activities [38,39]. This waste stream accounts for a significant portion, approximately 30–40 %, of the total solid waste generated globally [38]. Consequently, the scientific community has shown a growing interest in C&D waste, recognizing its potential for innovative solutions in waste management and environmental sustainability. In this framework, a recent review paper explores the application of adsorbents derived from C&D waste for eliminating contaminants from environmental settings, delivering threefold advantages in terms of waste treatment, solid waste management, and disposal [38]. However, while tuff and natural zeolites, in general, have been successfully tested for biogas purification [40,41], there is still a limited literature on their use as CO_2 adsorbents at low pressure. In this framework, Ammendola et al. [35,42,43] explored the adsorption of CO_2 at low pressures (<0.2 atm) on a naturally occurring tuff, with particular attention on both the thermodynamic and kinetic aspects of the process.

Aiming at improving the capture performances of natural zeolites, one viable solution consists in properly tailoring/modifying their structure (Si/Al ratio of the aluminosilicate framework) and chemical composition (nature of the extra-framework cations). Indeed, the degree/strength of adsorption within zeolitic pores is primarily influenced by the interactions between the adsorbate and the electric field induced by the cations [44]. It is also important to note that the acid-base properties of the zeolite framework can also play a vital role in determining adsorption characteristics, particularly under specific pressure conditions. In this context, the exchangeable cation acts as an acid site, while the framework oxygen nearest to the cation serves as a basic site. This basicity increases with higher framework aluminum content and also rises as the cation electronegativity decreases [44]. The strength of these zeolite acid-base pairs can be readily adjusted by cation-exchange or by modifying the aluminum content in the framework. In particular, the introduction of alkali metal ions (e. g. Na^+, Li^+, K^+, etc.) has been proved to lead to a notable enhancement in the CO_2 adsorption capacity of zeolites [45]. In this framework, Barthomeuf [46] observed that faujasites containing alkali metals (Li, Na, K, Rb, Cs) as charge compensating cations display an increase in basicity as the cation size increases. This is because the electronegativity of the cations affects the negative charge distribution on the oxygen atoms within the framework. Consequently, zeolites containing larger cations like Rb or Cs are expected to have greater capacities for acidic adsorbates, as long as steric limitations are not exceeded. However, it is worth noting that, when dealing with acidic molecules that also possess a quadrupole or permanent dipole moment, like CO_2, stronger interactions are anticipated with smaller cations such as Li. This is because smaller cations offer shorter interaction distances with the center of mass of the adsorbate. In summary, the interplay of cation type, acidity/basicity, and electrostatic interactions within zeolites is intricate and can vary depending on the specific characteristics of the adsorbates involved.

The objective of the current paper is, therefore, to further explore the application of zeolitic tuff derived from C&D waste in a CO_2 capture adsorption process, with the potential for direct operation on exhaust gases at CO_2 partial pressure. To achieve this goal, the tuff cation-exchange properties has been explored through the targeted introduction of different polar cations into its framework. The effect of several aspects has been investigated: cation nature (Na^+, which is already present in the raw tuff, and Li^+), amount of extra-framework cations, and preliminary treatment of the tuff to exchange it with NH_4^+ cations. In particular, the dynamic CO_2 adsorption capacity of untreated tuff as well as cation-exchanged tuff has been assessed in a fixed-bed reactor operated at ambient temperature (25 °C) and atmospheric pressure under a simulated flue gas stream containing a CO_2/N_2 mixture in typical industrial range (2–20 %vol. of CO_2 in N_2).

Experimental methods

Materials

The adsorbent material used in this work is a natural tuff derived from demolition of civil buildings in the Campania region of Italy. It was crushed and sieved to obtain a fraction with particle sizes ranging from 400 to 600 μm. Table 1 presents the main physical properties of this material [43].

Table 1
Physical properties of the natural tuff [43].

Particle size, μm	400–600
Particle porosity, -	0.339[a]
Absolute density, g mL^{-1}	2.241[a]
Tap density, g mL^{-1}	0.810
Specific heat, J g^{-1} K^{-1}	1.3
Minimum fluidization velocity, m s^{-1}	0.168

[a] Determined by MIP (mercury intrusion porosimetry).

Because of its naturally occurring state, the tuff contains several cations (Fe, K, Ca, Na, Mg [43]). To isolate the influence of individual cations, Na- (already present in the original framework) and Li-exchanged tuff samples were derived from the pristine tuff. The exchanged tuff samples were prepared by six consecutive cation-exchange cycles, using aqueous solutions of sodium chloride (NaCl) and Lithium chloride (LiCl). The tuff was washed with deionized water, filtered and dried overnight at 106 °C. Then, a typical cation-exchange cycle was performed by mixing 10 g of tuff powder 100 mL of 1 M cation salt solution. The mixture was stirred for 2 h in a bath at 60 °C. Following this, the solution was decanted, and fresh solution is added. This procedure was repeated six times. After the final exchange, the solution was filtered, washed with deionized water, and then dried in an oven at 106 °C. The samples were named Na-6 and Li-6, according to the nomenclature "c-n", where c is the exchanged cation and n the number of cation-exchange cycles.

Then, aiming at investigating the effect of the composition of extra-framework cations, two more Li-exchanged tuff samples were prepared, Li-3 and Li-9, by three and nine cation-exchange cycles.

Considering that replacing cations within the framework of natural zeolites is typically challenging in comparison to synthetic zeolite because of the strong cations/framework interaction [47], a common practice to enhance their exchange capacity involves an initial substitution with NH_4^+ ions. Therefore, two NH_4-exchanged tuff samples were prepared, NH_4-3 and NH_4-6, immersing the washed tuff in a 1 M aqueous solution of NH_4OH for 2 h in a bath at 60 °C for three and six consecutive exchange cycles, respectively. Then, after this preliminary step, these NH_4-exchanged samples were subsequently exchanged with Li^+ for three consecutive cycles to obtain the NH_4-3_Li-3 and NH_4-6_Li-3 samples. All the synthesized samples are summarized in Table 2.

Before performing the CO_2 adsorption study, the tuff samples were characterized from the physical and structural point of view:

- Scanning electron microscopy (Philips XL30 SEM-EDS) was employed for morphological characterization.
- XRD analysis was performed to determine the structure crystallinity and phase composition of the samples using a Bruker D8Advance powder diffractometer with CuKα radiation.
- The measurement of the specific surface area (SSA) and pore size distribution (PSD) (total pore volume, V_p and micropore volume, V_{micro}) was carried out by means of N_2 adsorption at 77 K in a Novatouch LX4 (Quantachrome instruments). In particular, the SSA was calculated using the Langmuir method, and the pore size distribution using the Density Functional Theory (DFT) method.
- The extent of cation-exchange, a crucial aspect for analyzing the cation effect in CO_2 adsorption, was determined by ICP-MS analysis (Agilent ICP-MS 7500ce spectrometer). In particular, prior to the analysis, 50 mg of the sample was mixed with 5 mL of deionized water and then digested using 5 mL of 65 % HNO_3 and 1 mL of 30 % H_2O_2, employing microwave heating for a duration of 30 min. Assuming that each cation can compensate the negative framework charges (AlO_4^-) depending on its positive charge (q), the cation exchange degree (CE_c) can be calculated as [48]:

$$CE_c = \frac{n_c}{n_{Al}/q} \times 100 \quad (1)$$

where n_c and n_{Al} are the number of moles, evaluated from the ICP-MS analysis, of the exchanged cation and of the aluminum in the sample framework, respectively. Considering that both Na^+ and Li^+ have one positive charge (i.e. monovalent cation, q = 1), each one of them can compensates one negative framework charges (AlO_4^-).

Table 2
Synthesized cation-exchanged samples.

	Exchanged cation	Number of exchange cycles
Na-6	Na^+	6
Li-3	Li^+	3
Li-6	Li^+	6
Li-9	Li^+	9
NH_4-3	NH_4^+	3
NH_4-6	NH_4^+	6
NH_4-3_Li-3	NH_4^+/Li^+	3/3
NH_4-6_Li-3	NH_4^+/Li^+	6/3

Experimental apparatus and CO_2 adsorption tests procedure

Experiments on the breakthrough of CO_2 adsorption were performed in a lab-scale fixed-bed reactor (ID = 1′, column length = 600 mm), depicted in Fig. 1, at atmospheric pressure. To regulate the temperature at the desired level, a PID controller was used in conjunction with an electric heating jacket (manufactured by Tyco Thermal Controls GmbH) and a type K thermocouple (with a diameter of 1 mm), employed to monitor the temperature. For each adsorption test, the gas feed was created by utilizing separate high-purity cylinders of N_2 and CO_2 (99.995 % vol.) and two mass flow-controllers (Brooks 8550S) to adjust and monitor the inlet flowrates.

The continuous gas analyzer, equipped with an infrared detector (ABB AO2020, URAS 14), was used to monitor the adsorption process and measure the outlet CO_2 concentration. Before starting the adsorption, the sorbent (5 g, equivalent to around 5 cm of bed height) was subjected to a drying/cleaning step, during which N_2 (15 L h^{-1}) was flowed through the bed for 60 min at 150 °C and atmospheric pressure to eliminate water that may hamper CO_2 adsorption efficiency. Once the sorbent was dried and cleaned, it was subjected to a pre-conditioning step at the desired adsorption temperature (T = 25, 70, 100 and 150 °C), where N_2 is flowed through the bed at a rate of 15 L h^{-1} until the set temperature was reached. The CO_2 adsorption process was then initiated by introducing a 15 L h^{-1} CO_2/N_2 gas mixture with varying CO_2 concentrations (2, 3, 5, 10, 15, and 20 % vol.) into the column. The breakthrough curves were obtained by continuously monitoring the CO_2 concentration in the outlet stream until the bed became saturated, which was indicated by the outlet CO_2 concentration approaching the inlet value.

For every CO_2 adsorption test, a breakthrough curve was generated, which is a plot of C/C_0 versus time, where C and C_0 are the volumetric CO_2 concentrations in the outlet and inlet stream, respectively. Using

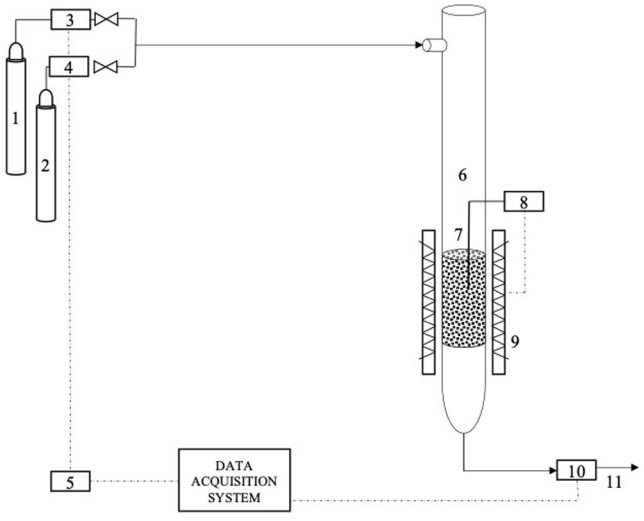

Fig. 1. Experimental apparatus: 1) N_2 cylinder; 2) CO_2 cylinder; 3) N_2 mass flow-controller; 4) CO_2 mass flow-controller; 5) multichannel control instrument; 6) 1′ ID fixed-bed reactor; 7) thermocouple; 8) temperature controller; 9) heating jacket; 10) CO_2 analyzer; 11) stack.

this data, crucial adsorption parameters were calculated [5,49,50]:

i) The quantity of CO_2 adsorbed per unit mass of adsorbent, q_e (i.e. equilibrium adsorption uptake at each CO_2 partial pressure), was determined by integrating the breakthrough curves applying a mass balance equation to the adsorption column

$$q_e = \frac{1}{m}\int_0^{t_s} \left(F_{CO_{2,in}} - F_{CO_{2,out}}\right) dt \quad (2)$$

and knowing the mass of sorbent in the bed (m), the molar flowrate of CO_2 at the inlet ($F_{CO2,in}$) and outlet ($F_{CO2,out}$) of the bed, and the time needed to saturate the bed of sorbent (t_s).

ii) The breakthrough time, t_b, is the time at which the outlet CO_2 concentration reaches 5 % of the inlet concentration. It is also the time when the reactor is shut down for regeneration. A higher t_b corresponds to a higher effective capture capacity.

iii) The fraction of bed used at breakpoint, denoted as W, represents the percentage of CO_2 adsorbed until t_b in relation to the total amount of CO_2 adsorbed when the bed is completely saturated.

iv) The time parameter $\Delta\tau = t_{70} - t_{10}$, where t_{10} and t_{70} represent the times at which CO_2 reaches 10 % and 70 % of the inlet concentration at the adsorption column outlet, is closely associated with the slope of the linear portion of the sigmoid-shaped breakthrough curve. Smaller $\Delta\tau$ values indicate a steeper breakthrough curve and, consequently, faster adsorption. Indeed, a sharpest curve implies that the saturation adsorption capacity is reached more quickly, which means that, at a fixed CO_2 adsorption capacity, a shorter length of the bed remains unused before the breakthrough occurs.

Following each adsorption step, the sorbent underwent regeneration through the temperature swing adsorption (TSA) method. Upon reaching saturation, the column was heated to 150 °C, and N_2 (15 L h^{-1}) was flowed through the heated sorbent bed. The multi-cyclic stability of the synthesized sorbents was evaluated through 10 consecutive adsorption/desorption cycles.

Adsorption isotherms

Adsorption isotherms, which are graphical representations of the relationship between the equilibrium CO_2 uptake and CO_2 partial pressure at a fixed temperature, describe the adsorption equilibrium [51]. In particular, the equilibrium CO_2 uptake (q_e) for a certain temperature and CO_2 partial pressure was calculated by integrating the breakthrough curves (Eq. (2), as described in paragraph 2.2.

According to the results obtained in a previous work on the natural tuff [43] and, also, in line with most of the studies available on CO_2 adsorption on physical sorbents such as activated carbons and zeolites [37–45], the Freundlich model [52] was used to fit the experimental adsorption isotherms of the different synthesized tuff samples. Indeed, in practice, it is rare to observe adsorption of molecules on surfaces with a constant energy of interaction, which contradicts the assumption made by Langmuir. This is because most solids exhibit high levels of heterogeneity, which can be commonly accounted for assuming that that the energy of interaction between molecules and surfaces adheres to a mathematical distribution. More specifically, non-ideal multilayer adsorption, which can occur when several layers of adsorbate attach to the adsorbent (also characterized by surface heterogeneity), can be suitably described by the Freundlich model [53,54]. This model, in particular, assumes an exponential decrease in the adsorption energy as the number of available adsorption sites decreases, which happens with increasing surface coverage. Its mathematical expression is [52]:

$$q_e = K_F {P_{CO_2}}^{1/n} \quad (3)$$

The parameters of the model are the Freundlich isotherm constant (K_F), whose units are mmol g^{-1} $atm^{-1/n}$, and the dimensionless heterogeneity factor (n, Freundlich coefficient). The Freundlich intensity parameter, given by the ratio 1/n, is a measure of the binding energy between the adsorbate and adsorbent and the heterogeneity of the surface. Whether the adsorption process is favorable or not can be inferred from the magnitude of 1/n: it is favorable when $1/n < 1$ [52].

To evaluate the quality of the isotherm fit using the Freundlich model, two parameters are commonly used: the coefficient of correlation, R^2, which ranges from 0 to 1, and the HYBRID error function. The HYBRID error function, defined in Eq. (4), was introduced to enhance the fitting quality of the sum of squares of errors (SSE) method at low partial pressure values [55]. The lower the HYBRID value, the better the fitting quality.

$$HYBRID(\%) = \frac{100}{n-p}\sum_{i=1}^{i=n}\left[\frac{\left(q_{mod_i} - q_{exp_i}\right)^2}{q_{exp_i}}\right] \quad (4)$$

In Eq. (4), q_{exp} and q_{mod} are the adsorption uptakes experimentally and theoretically evaluated, respectively, p and n are the number of parameters of the equation and the number of experimental points.

A crucial factor when studying the adsorption process is the isosteric heat of adsorption (Q_{st}) [56], which is the heat of adsorption at a constant amount of adsorbed adsorbate. This parameter serves as an indicator of the strength of molecular-scale interactions between the adsorbate molecules and the adsorbent surface. Typically, Q_{st} values below 80 kJ mol^{-1} indicate physisorption, while values in the range of 90–100 kJ mol^{-1} suggest strong chemisorption [54,57,58]. Furthermore, details about its magnitude and variation with surface coverage serve as criteria for assessing the energetic heterogeneity of a solid surface [54,57,58]. Specifically, Q_{st} remains constant with surface coverage in the absence of interactions among adsorbed molecules, indicating surface homogeneity [54,57,58]. In contrast, a change in Q_{st} with surface loading suggests varying levels of surface energy and heterogeneity on the adsorbent surface [54,57,58]. The calculation of Q_{st} at a particular adsorbed CO_2 amount involves integrating the Clausius–Clapeyron equation. This is achieved by utilizing the slopes derived from the plot of $\ln PCO_2$ against 1/T at a fixed and specified adsorbed quantity of CO_2, commonly referred to as the slopes of adsorption isosteres [35,51,58].

The N_2 adsorption isotherm at ambient temperature (25 °C) of Li-9, namely the top-performing sample, was also obtained using a 3Flex adsorption analyzer (Micromeritics) in order to evaluate its CO_2/N_2 selectivity. Prior to measurement, the sample underwent a 12-hour degassing process under vacuum conditions at 150 °C. The CO_2/N_2 selectivity factor (S_{CO_2/N_2}) was estimated measuring the equilibrium capacities of pure fluids, i.e. CO_2 and N_2. Specifically, it was calculated as the ratio between the equilibrium adsorption uptakes (q_e) of CO_2 and N_2 at given relative pressures (i.e. for a specified CO_2/N_2 mixture), obtained from the respective single-component isotherms [59]:

$$S_{CO_2/N_2} = \frac{q_{CO_2}/P_{CO_2}}{q_{CO_2}/P_{N_2}} \quad (5)$$

where q_{CO2} and q_{N2} are the adsorbed amount of CO_2 and N_2, respectively, P_{CO2} is the partial pressure of CO_2 and P_{N2} the partial pressure of N_2 (i.e. 1 - P_{CO2}) in the CO_2/ N_2 mixture.

Results and discussion

Materials characterization

Fig. 2 reports the SEM images obtained for the tuff and all the cation-exchanged samples. Overall, the material exhibits micronic cubic-shaped structures, which are characteristic of zeolites, along with glassy regions [35]. The microstructure of the untreated tuff seems denser compared to samples with substituted cations. Specifically, those

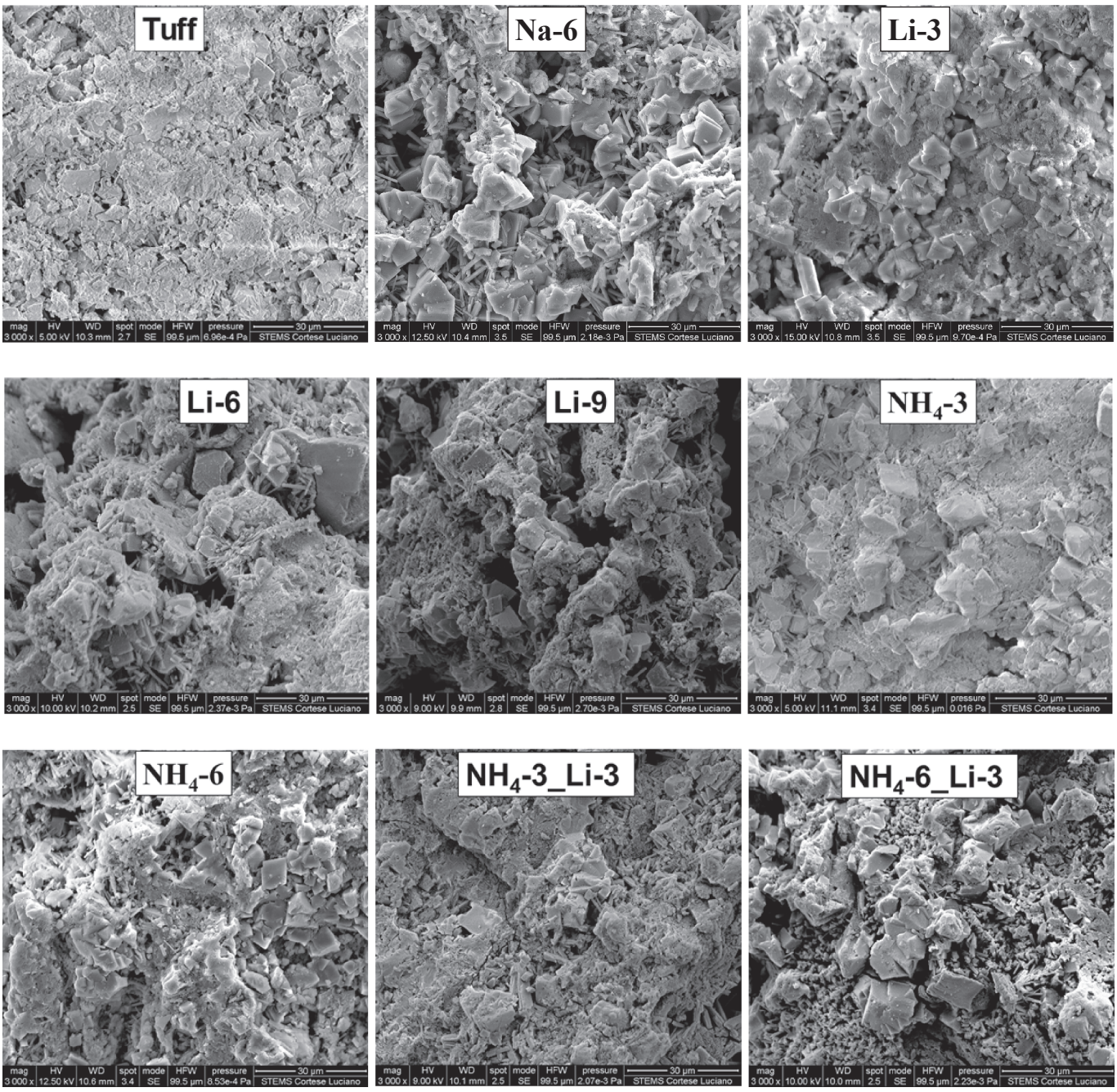

Fig. 2. SEM images at different magnification of tuff and ion exchanged samples.

exclusively exchanged with Li and Na exhibit noticeable macroporosity, characterized by the presence of weakly connected cubic structures to the main material body.

Fig. 3 displays the XRD patterns of the samples. The natural tuff demonstrates pronounced crystallinity, featuring distinctive reflection peaks of chabazite at 2θ = 9.45, 12.84, 13.89, 15.99, 17.61, 20.51, 22.97, 24.73, 25.82, 30.63, and 30.73° [60], commonly found in natural zeolites, alongside various other impurities, among which primarily feldspar (2θ = 23.45, 25.83, 27 – 28°) and quartz (2θ = 26.6°). Comparison of the XRD patterns between the cation-exchanged samples and the pristine tuff shows that the fundamental crystalline structure, particularly that of chabazite, has been preserved. No novel diffraction peaks have emerged in the samples, indicating the crystal structure stability. Nonetheless, a slight reduction in the intensity of certain characteristic peaks, such as those of quartz and feldspar, has been observed. This subtle shift can be ascribed to alterations in the chemical composition of the sample resulting from the ion-exchange process.

The surface analysis results, presented in Table 3, reveal a relatively low SSA (36 $m^2\ g^{-1}$) for the tuff, consistent with values reported for other natural tuffs [61,62]. With reference to the porosimetric analysis (Fig. 4 and Table 3), the tuff exhibits a pronounced peak in the differential pore size distribution at approximately 1.9 nm, indicating a certain concentration of these micropores within the tuff. Besides, the rapid rise and plateau in cumulative pore volume suggest that the material has a high proportion of small micropores with less contribution from larger pores (54 % of the total pore volume is ascribable to micropores, i.e. smaller than 2 nm).

Passing to comparing the textural properties of the cation-exchanged samples with those of the pristine tuff, the results obtained show that the pore structure of all the synthesized samples can be altered to varying

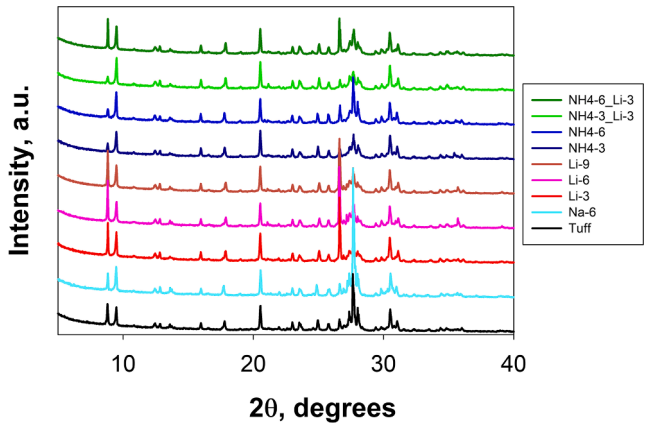

Fig. 3. XRD patterns of tuff and ion exchanged samples.

Table 3
SSA and pore volume of the analyzed samples.

	SSA $m^2\ g^{-1}$	V_p $10^{-2}\ cm^3\ g^{-1}$	V_{micro} $10^{-2}\ cm^3\ g^{-1}$
Tuff	36	2.13	1.15
Na-6	81	3.94	3.05
Li-9	155	5.78	5.05
NH_4-6	7	1.39	0.85
NH_4-6_Li-3	63	4.07	1.87

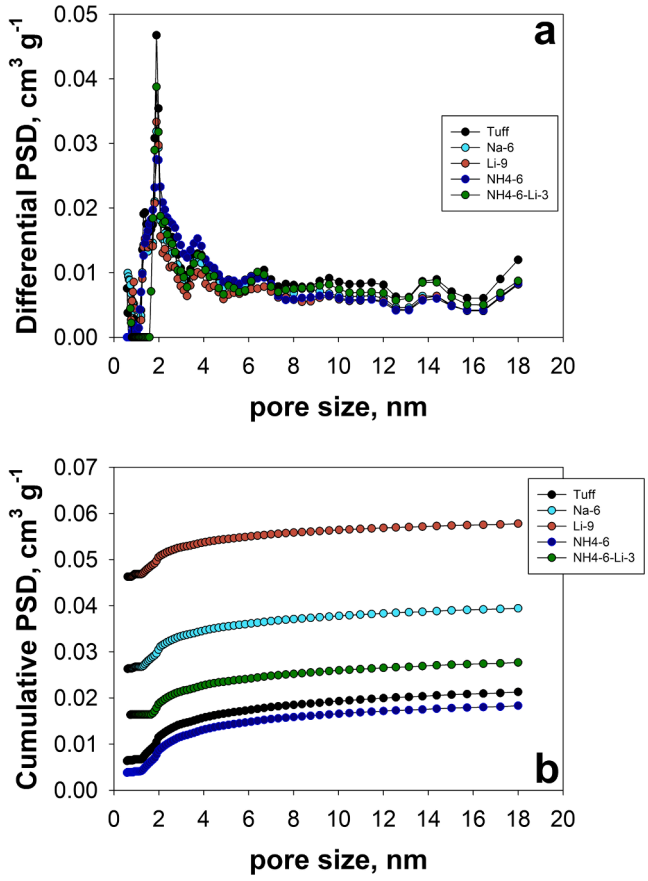

Fig. 4. Differential (a) and cumulative (b) pore size distributions of tuff and ion exchanged samples.

extents, depending on the specific treatment. Specifically, when the tuff is exchanged with either Li^+ or Na^+ (Li-9 = 155 m^2/g; Na-6 = 81 $m^2\ g^{-1}$); namely an increase by over fourfold and twofold, respectively, with respect to the untreated tuff (36 $m^2\ g^{-1}$). Referencing to the porosimetric analysis, both Li-9 and Na-6 show a similarly elevated peak in the differential pore size distribution at approximately 1.9 nm. However, their cumulative pore volume profiles rise more smoothly and reach a higher plateau than the untreated tuff. This indicates an overall enhancement in their porosity due to the cation-exchange. More specifically, both Li-9 and Na-6 are characterized by a greater portion of micropore with respect to the untreated tuff; 87 and 77 % of their total porosity, respectively, can be attributed to small micropores (smaller than 2 nm). Moreover, it is also noteworthy that the increase of their total pore volume, and in turn of their SSA, is almost exclusively due to an enhancement of their microporosity compared to the pristine tuff. Indeed, it can be inferred that, while the volume of mesopores remains almost unchanged with respect to the original tuff, their microporosity experiences a substantial expansion, increasing more than fourfold and twofold, respectively. These results are in line with the enhancement of microporosity observed for other Li and Na-exchanged of zeolites [63]. On the contrary, it can be observed that the exchange with NH_4^+ is quite inefficient in enhancing the textural properties of the tuff. Indeed, the NH_4-exchanged sample, i.e. NH_4-6, continues to exhibit the inherently low SSA and pore volume typical of the pristine tuff. This outcome highlights the crucial impact of cation size on the pore architecture. The different behavior between all the cation exchanged samples can be, indeed, ascribed to the ionic radii of the different elements used in the tuff exchange process (Li^+ = 0.68 Å; Na^+ = 0.97 Å; NH_4^+ = 1.4 Å [45]). Particularly, the smaller sizes of Li^+ and Na^+ allow them to occupy less volume compared to the larger NH_4^+, leading to an enhanced porous volume that is not achievable with the NH_4^+ exchange. Finally, the outcome for NH_4-6_Li-3 (63 $m^2\ g^{-1}$), representing the sample first exchanged with NH_4^+ and then with Li^+, aligns with the above-described impact of differently sized cations. Specifically, introducing Li^+ into the NH_4-6 sample framework significantly boosts its SSA and V_p, compared to NH_4-6 (7 $m^2\ g^{-1}$). This improvement is a result of replacing the larger NH_4^+ cations with the smaller Li^+ cations, which effectively creates additional pore volume within the material.

The results of the ICP-MS analysis and the values of cation exchange degree, CE_c (with c being either Li, Na or both of them), of all the exchanged samples are reported in Table 4. Firstly, it can be observed that the Li-exchange is generally linked to a notable decrease of Na with respect to the pristine tuff (Table 4), showing that the introduction of Li in the tuff framework occurs at the expense of the original Na content, even though a slight reduction of K content has also been observed (i.e. Li cations mostly replace Na cations). On the contrary, in the case of the Na-exchanged sample (Na-6), it has been observed that the increasing amount of Na in the tuff framework occurs at the expense of different cations, namely K, Ca, Fe and Mg.

The value of CE_{Na} reported for the untreated tuff represents a just a

Table 4
Results of ICP-MS and CE of all the synthesized cation-exchanged samples.

	Na %wt	Li %wt	Al %wt	CE_{Li} %	CE_{Na} %	Li/Na* -	$CE_{(Li+Na)}$ %
Tuff	2.1	–	9.8	0.0	25.1**	–	25.1
Na-6	4.0	–	6.9	0.0	68.7	–	68.7
Li-3	1.3	0.5	10.4	18.4	15.1	1.2	33.5
Li-6	1.1	1.3	10.7	46.0	9.9	4.6	55.9
Li-9	0.7	1.9	11.3	63.5	6.8	9.4	70.3
NH_4-3	1.9	–	10.3	0.0	21.4	–	17.6
NH_4-6	1.8	–	10.1	0.0	21.2	–	15.8
NH_4-3_Li-3	1.3	0.5	10.5	17.4	14.2	1.2	31.5
NH_4-6_Li-3	1.2	0.5	10.5	16.7	13.8	1.2	30.5

*molar fraction.
**theoretical CE_c.

theoretical cation exchange degree; specifically, the percentage of framework where negative charges are compensated by the Na inherently present in the pristine tuff. Based on the results in Table 4, it can be observed that, for the same number of cation-exchange cycles, the amount of cation that can be inserted is independent of the cation nature, whether it is Na or Li (i.e. cation-exchange performed in aqueous solutions of either NaCl or LiCl). Indeed, in both Na-6 and Li-6 the six cation-exchange cycles result in an approximately 45 % increase in the compensation of the negative framework charges (AlO_4^-) from either Na or Li. CE_{Li} of Li-6 is 46 % and the CE_{Na} of Na-6 is 68.7, corresponding to a variation of CE_{Na} with respect to the original tuff of 44 %. However, it must be noted that when considering both cations, Li-6 (55.9 %) is less exchanged compared to the Na-6 (68.7 %) on an overall basis.

The effect of the number of cation-exchange cycles has been assessed by preparing Li-exchanged samples at three and nine cycles, denoted as Li-3 and Li-9, respectively. It can be inferred that increasing the number of consecutive cation-exchange cycles leads to a progressive rise in the Li content within the tuff and a corresponding reduction of the remaining Na cations; a less evident gradual reduction of K content has also been observed. Specifically, the Li-exchange degree goes from 18.4 % in Li-3 (Li/Na = 1.2), with three cation-exchange cycles, up to 63.5 % in Li-9 (Li/Na = 9.4), which has undergone nine cation-exchange cycles.

It is also important to highlight that, despite a reduction in the Na content, the overall cation exchange degree, $CE_{(Li+Na)}$, which accounts for the overall compensation of the negative framework charges resulting from both Na and Li, tends to rise as the number of Li-exchange cycles increases, going from 33.5 up to 70.3 %.

With reference to the cation exchange pre-treatment performed in NH_4OH aqueous solution, it is evident that it results in a slight reduction of the Na content, also accompanied by a minor decrease in K content. Indeed, NH_4-3 and NH_4-6, prepared with three and six cation-exchange cycles, respectively, experience a reduction of about 10 and 13 % in their Na content with respect to the pristine tuff (corresponding to a CE_{Na} of 17.6 and 15.8 %).

Finally, the possibility to enhance the cation-exchange capacity of natural zeolites with a previous substitution with NH_4^+ cations has been assessed subjecting the NH_4-exchanged samples to three consecutive Li-exchange cycles, thus obtaining the NH_4-3_Li-3 and NH_4-6_Li-3 samples. However, it can be clearly observed that this preparation results in the same Li content (Li = 0.5 %wt, corresponding to a CE_{Li} of about 17 %) as compared to Li-3 (Li = 0.5 %wt, corresponding to a CE_{Li} of about 18 %), namely the Li-exchanged sample that has not undergone the pre-treatment. Therefore, in the case of the natural tuff examined in this study, NH_4^+ cations do not affect the Li^+ incorporation.

CO_2 adsorption tests

The breakthrough curves derived from the dynamic adsorption tests was elaborated in order to obtain: the adsorption isotherms, the values of breakthrough time (t_b), the time parameter ($\Delta\tau$), and the fraction of bed used at t_b (W). Fig. 5 reports the breakthrough curves obtained for a CO_2 inlet concentration of 10 %vol. and a temperature of 25 °C; similar trends were obtained at all the other tested inlet CO_2 concentrations and temperatures.

Significantly, it is noteworthy that Li-9 demonstrates the longest breakthrough time, approximately 5 min, while Na-6 exhibits the sharpest-shaped profile. The adsorption isotherms, obtained at 25 °C, which was fitted using the Freundlich model, and all the evaluated parameters, t_b, $\Delta\tau$ and W, as functions of P_{CO2} are reported in Fig. 6 and Fig. 7, respectively. Similar trends were obtained at all the other tested inlet CO_2 concentrations and temperatures Table 5 presents the value of the CO_2 adsorption capacity (denoted as q_e) obtained for all the samples at the different tested CO_2 partial pressure. Table 6 provides the values of the model parameters along with the values of R^2 and HYBRID.

With reference to Fig. 6, the experimental data points are represented by markers, while the solid lines correspond to the outcomes of

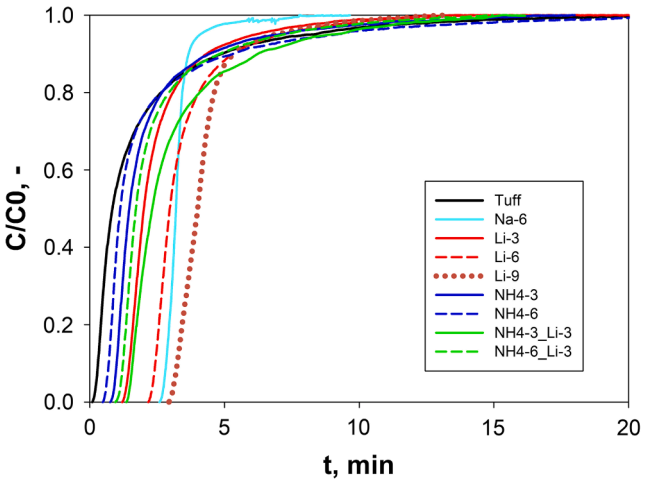

Fig. 5. Breakthrough curves for CO_2 adsorption on all the samples (C_0 = 10 % vol; T = 25 °C).

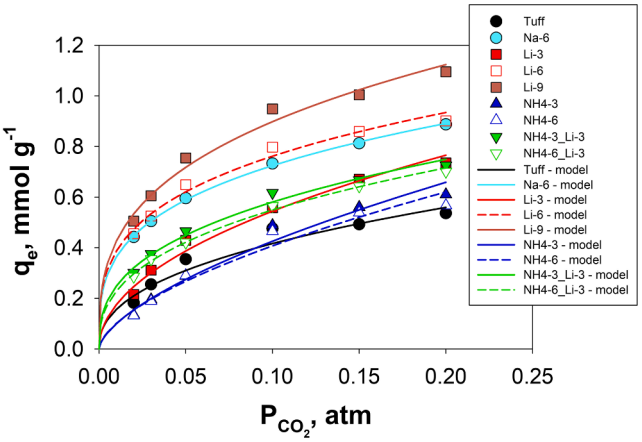

Fig. 6. CO_2 adsorption isotherms obtained for all the samples and fitted by the Freundlich model (T = 25 °C).

the isotherm model.

It is evident, from Fig. 6 and Table 5, that the CO_2 adsorption capacity (namely the quantity of CO_2 adsorbed at the thermodynamic equilibrium) increases as P_{CO2} is raised; this aligns with the notion that, from a thermodynamic standpoint, P_{CO2} serves as the driving force for the adsorption process.

From a kinetic perspective, P_{CO2} positively impact the CO_2 adsorption rate. Indeed, the adsorption process becomes faster, meaning that the time required to reach the equilibrium decreases and the breakthrough curves become progressively steeper with higher values of P_{CO2}. This is evident from the reduction of $\Delta\tau$ and the increase of W as P_{CO2} is increased (Fig. 7b and c). This observed result can be explained considering that, when P_{CO2} is increased, the adsorption process speeds up, primarily due to an enhanced mass transfer rate resulting from the increased adsorption driving force [64]. Lower values of P_{CO2}, on the contrary, slow down the adsorption process (i.e. slower breakthrough curves) because the CO_2 concentration front requires a longer time to reach the column outlet [5,65,66]. This observation aligns with findings reported in various studies that employ physical sorbents for CO_2 capture [5,65,66].

As regards the breakthrough time, t_b, it is adversely impacted by the CO_2 partial pressure; indeed, regardless of the specific sample, it decreases when P_{CO2} is increased (Fig. 7a). This result stems from the interplay of two contrasting phenomena:

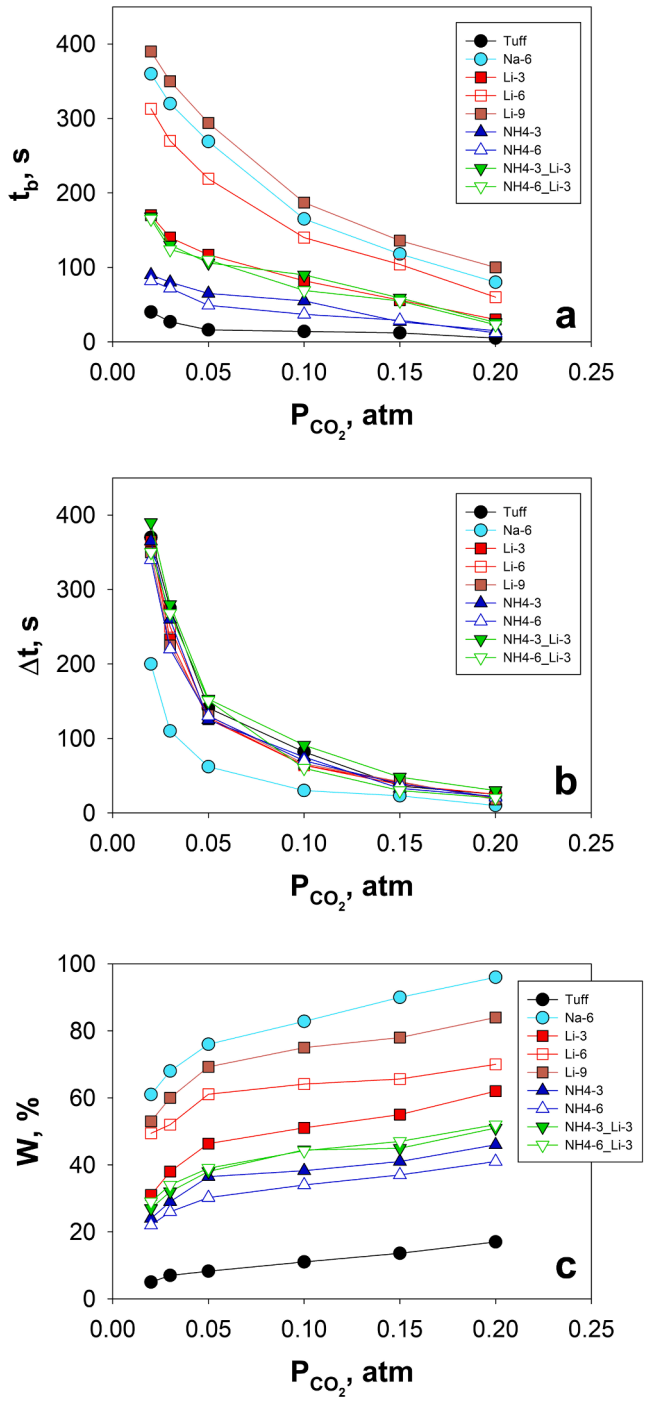

Fig. 7. Breakthrough time (a), t_b, time parameter (b), Δτ, and fraction of bed utilized at t_b (c), W, as functions of the CO_2 partial pressure (P_{CO2}) for all the samples.

a. From a thermodynamic perspective, higher values of CO_2 partial pressure lead, indeed, to an increased sorbent adsorption capacity, as stated above, thereby tending to prolong the breakthrough time. Anyway, the dependence of CO_2 capacity on P_{CO2} is less than linear (Fig. 4).
b. Conversely, from a kinetic perspective, increased P_{CO2} levels accelerate the adsorption process by increasing the process driving force, resulting in the sorbent being more quickly saturated and, consequently, in t_b tending to be also decreased.

As a consequence of these opposite influences, the net result is that t_b decreases with increasing P_{CO2}. This means that the impact of P_{CO2} on accelerating the adsorption process ("kinetic effect") prevails over its effect on increasing the adsorption capacity ("thermodynamic effect").

Form the analysis of Fig. 6 and Table 6 it can be clearly inferred that the model provides a good fit to the experimental results, consistent with findings on physical sorbents obtained by other researchers [55,67–74]. This is further substantiated by the fact that R^2 consistently exceeds 0.98, and HYBRID consistently remains below 0.5 %. Furthermore, concerning the outcomes derived from the Freundlich model, it is noteworthy that the values of n consistently exceed 1 for all the samples. This observation suggests a high level of energetic heterogeneity of the solid surface as well as a strong intensity of adsorption [52,75,76], which is in line with the results reported for tuff and other natural zeolites [43,77].

Fig. 8 shows the isosteric heat of adsorption (Q_{st}), evaluated for all the samples, as a function of the equilibrium surface loading. The magnitude and variation of Q_{st} during CO_2 adsorption, specifically with increasing surface loading, offer insights into the molecular-scale interactions between CO_2 molecules and the adsorbent and also sheds light on the energetic heterogeneity of the solid surface [54]. Primarily, it can be inferred that all the samples exhibit Q_{st} values ranging between 11-20 and 30–65 kJ mol^{-1}, indicative of a purely physical interaction (< 80 kJ mol^{-1}) [69] and in line with the results reported in the literature on similar materials [78]. This consistency across samples suggests that the adsorption process, regardless of cation exchange or the introduction of different ions, is primarily governed by physical forces such as Van der Waals interactions, hydrophobicity, and other physisorption mechanisms [79]. Nonetheless, it is noteworthy that the exchanged samples exhibit larger values of Q_{st} with respect to the pristine tuff (Fig. 8). This finding underscores an enhanced interaction between CO_2 molecules

Table 6
Freundlich adsorption equation parameters and fitting comparison (T = 25 °C).

	K_F mmol g^{-1}	n	1/n -	R^2 -	HYB. %
Tuff	1.110	2.348	0.426	0.986	0.459
Na-6	1.441	3.345	0.299	0.999	0.007
Li-3	1.690	2.031	0.492	0.995	0.269
Li-6	1.501	3.391	0.295	0.998	0.124
Li-9	1.890	3.093	0.323	0.997	0.180
NH4-3	1.815	1.587	0.630	0.988	0.391
NH4-6	1.648	1.646	0.607	0.985	0.458
NH4-3_Li-3	1.355	2.714	0.368	0.997	0.122
NH4-6_Li-3	1.321	2.621	0.381	0.999	0.034

Table 5
Equilibrium CO_2 adsorption capacity (q_e) obtained at different P_{CO2} and T = 25 °C.

P_{CO2}	Tuff	Na-6	Li-3	Li-6	Li-9	NH4-3	NH4-6	NH4-3_Li-3	NH4-6_Li-3
0.02	0.182	0.442	0.215	0.455	0.505	0.135	0.132	0.301	0.286
0.03	0.255	0.505	0.311	0.525	0.605	0.195	0.189	0.375	0.355
0.05	0.354	0.595	0.429	0.649	0.754	0.288	0.290	0.465	0.421
0.10	0.476	0.732	0.558	0.797	0.948	0.488	0.466	0.617	0.565
0.15	0.492	0.812	0.671	0.859	1.004	0.560	0.538	0.667	0.643
0.20	0.536	0.887	0.735	0.901	1.095	0.610	0.567	0.725	0.701

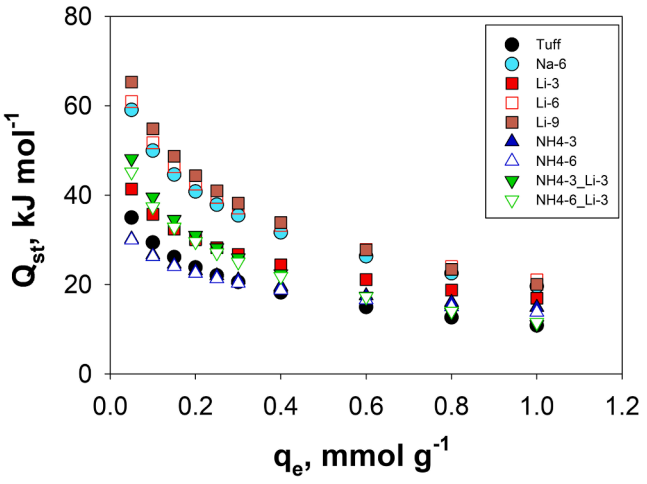

Fig. 8. Isosteric heat of adsorption (Q_{st}) as a function of the CO_2 surface loading for all the synthesized samples.

and the sorbent surface achieved through the cation-exchange modification.

Then, it is evident that Q_{st} decreases with a rise in CO_2 surface loading, indicating the high heterogeneity of the samples and a variation in adsorbate-adsorbent and adsorbate–adsorbate interactions [80]. During the initial stages of adsorption, numerous free adsorption sites are accessible on the surface of the samples. Consequently, CO_2 molecules can readily make direct contact with the adsorbent surface, leading to more intense forces between CO_2 molecules and the adsorbent. As a result, the activation energy is low, and the heat of adsorption is high. As the adsorption process progresses, with an increase in surface coverage, fewer adsorption sites remain available. Consequently, the adsorption of additional CO_2 molecules becomes increasingly challenging. Moreover, with rising surface coverage, adsorbate–adsorbate interactions become significant. This suggests the presence of lateral interactions in the adsorbed layers, encompassing attractive/repulsive London dispersion intermolecular forces among adsorbed CO_2 molecules [80–82]. Consequently, with the progression of the adsorption process, there is an increase in activation energy and a decrease in the heat of adsorption [83,84].

The results obtained from the adsorption tests clearly evidenced that both the Na- and Li-exchanged samples exhibit better CO_2 adsorption performances as compared to the pristine tuff, with Na-6 and Li-6 equilibrium adsorption capacities reaching values as high as approximately 0.9 mm g^{-1} at a CO_2 partial pressure of 0.2 atm (an increase of about 80 % with respect to the pristine tuff). More specifically, Na-6 and Li-6 are characterized by nearly identical adsorption isotherms, with a slight advantage in favor of Li-6 within the range of 3-9 %. However, it is important to underline that, when considering the overall cation-exchange degree, i.e. $CE_{(Li+Na)}$, Li-6 (55.91 %) is globally exchanged to a lesser extent than Na-6 (68.71 %). Nonetheless, it exhibits slightly superior CO_2 adsorption performances, thus evidencing that Li-exchange is slightly more effective than the Na-exchange in enhancing the CO_2 adsorption performances of the studied tuff. This result can be elucidated by considering the interaction between the quadrupole moment of CO_2 molecules and the electrostatic field of the tuff, as suggested in [85]. Despite the larger Na cations contributing to greater basicity in the tuff framework, the smaller Li cations offer a significantly higher electrostatic field intensity, particularly in terms of the charge density. This ultimately leads to a much stronger ion–quadrupole interaction, and therefore higher CO_2 adsorption energy, in the case of Li-exchanged tuff [45]. This result is also confirmed by the larger isosteric heat of the Li-exchanged samples with respect to the Na-exchanged samples (Fig. 8), which testifies the stronger interaction between CO_2 and the Li^+ cations compared to Na^+ cations. It is also worth mentioning that the observed variation of Q_{st} follows the same sequence as the basicity of the samples ($Li^+ < Na^+$), as typically observed for alkali-exchanged zeolites [86]. Likewise, the NH_4-exchanged samples are characterized by values of Q_{st} very comparable to the untreated tuff, in line with the observed similar CO_2 adsorption performances.

With reference to the effect of the composition of extra-framework cations, it can be inferred that increasing amount of Li inside the framework has a beneficial effect on the CO_2 adsorption performances. Indeed, increasing the Li-exchange degree from 18.42 %, in Li-3 (Li/Na = 1.22, with 3 cation-exchange cycles) up to 63.53 % in Li-9 (Li/Na = 9.36, with 9 cation-exchange cycles), the amount of CO_2 adsorption can be enhanced by approximately 50 % to 135 %, depending on the CO_2 partial pressure. It is also noteworthy that at same overall percentage of cation-exchange, i.e. $CE_{(Li+Na)}$ of about 70 %, the sample with Li as the dominant cation, Li-9, exhibits better adsorption performances (approximately 30 % improvement) than the Na-enriched tuff, Na-6. This result is also in line with the superior textural properties (SSA and pore volume) exhibited by Li-9 with respect to Na-6.

Regarding the NH_4-exchanged samples, it can be observed that the adsorption behavior of both NH_4-3 and NH_4-6 is quite similar to that of the untreated tuff (Fig. 6 and Table 5). This result can be attributed to their comparable textural characteristics to the original tuff, namely, the relatively low specific surface area and micropore volume. Likewise, in line with the evidence that the previous substitution with NH_4^+ cations has practically no impact on the ultimate amount of Li in the framework as compared to the corresponding Li-exchanged sample that has not undergone pre-treatment, NH_4-3_Li-3 and NH_4-6_Li-3 are characterized by CO_2 adsorption isotherms entirely similar to that of Li-3.

The multi-cyclic stability of the synthesized sorbents has been evaluated carrying out 10 consecutive adsorption/desorption cycles. The results obtained, in terms of equilibrium CO_2 adsorption capacity (q_e) over increasing number of cycles (n), are reported in Fig. 9. Regardless of the specific cation-exchange type, the adsorption performances of all the synthesized samples remain constant over all the cycles, aligning with the inherent stability observed in zeolitic materials commonly used as physical sorbents [87]. This result underscores the robust reliability and durability of the synthesized samples as potential candidates for applications requiring repeated adsorption/desorption cycles.

Fig. 10 shows the N_2 adsorption isotherm obtained at 25 °C for Li-9, i.e. the top-performing ion-exchanged sample. Clearly, CO_2 is adsorbed in a much larger amount than N_2, ranging from a selectivity factor of 187 for a 2 %/98 % CO_2/N_2 mixture down to 40 for a 20 %/80 % CO_2/N_2 mixture. This is in line with results reported on zeolites in general and chabazite-like zeolites, that are widely recognized to be excellent molecular sieves capable of separating CO_2 (3.3 Å) from N_2 (3.6 Å) in flue gases [88]. Besides, these values of selectivity are larger than those reported for both zeolites [86,87] and other types of sorbents, such as

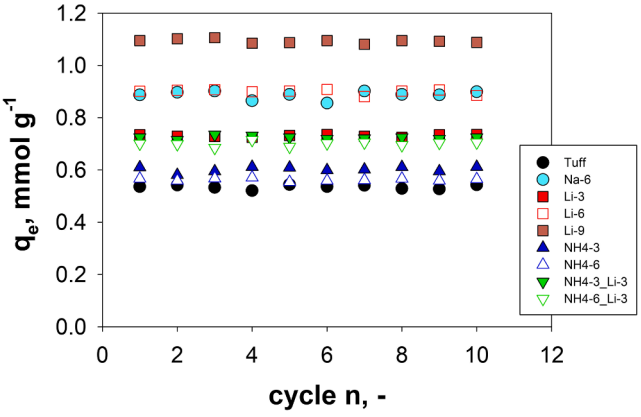

Fig. 9. Equilibrium CO_2 adsorption capacity (q_e) of all the samples vs the number of cycles (n). T = 25 °C (Adsorption); 150 °C (Regeneration).

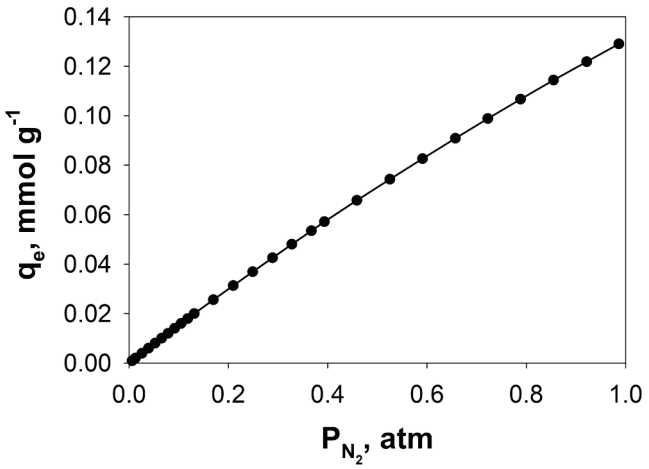

Fig. 10. Adsorption isotherm of N_2 on Li-9 obtained at 25 °C.

activated carbons [24] and MOFs [59].

Conclusions

This work explores the critical role of cation-exchange processes in enhancing the CO_2 adsorption capabilities of natural tuff, derived from construction and demolition (C&D) waste, for effective post-combustion capture of CO_2 from industrial flue gases. In particular, the experimental investigation, carried out in a fixed-bed reactor at low CO_2 partial pressure (< 0.2 atm), examines the dynamic adsorption capacity of both untreated and cation-exchanged tuff. Key conclusions drawn from the experimental outcomes include:

1. Impact of cation species
- Textural properties - The analyses of surface texture and porosity highlight the profound impact of cation exchange on the tuff's textural features, especially concerning changes in microporosity and specific surface area (SSA). The extent of these modifications is largely determined by the size of the cation, emphasizing the intricate relationship between ion exchange and material characteristics, as well as the critical role of cation selection for tailored applications. Notably, ion exchange with Li^+ and Na^+ markedly increases both SSA and microporosity, demonstrating the potential for improved CO_2 capture performance.
- Li-exchange superiority - Despite a lower overall cation exchange degree, Li-exchanged tuff (Li-6) surpasses Na-exchanged tuff (Na-6) in the CO_2 adsorption capacity. This result is ascribed to the enhanced ion–quadrupole interaction facilitated by Li higher electrostatic field intensity. This superiority is also confirmed at fixed overall CE_c (about 70 %); indeed, Li-9 is characterized by better adsorption performances than Na-6, which is also in line with its superior textural properties (SSA and pore volume) with respect to Na-6.
- Ineffectiveness of NH_4^+ pre-treatment – ion exchange with NH_4^+ fails in improving the textural properties of the tuff; NH_4-exchanged samples keep the characteristically poor textural properties of the pristine tuff, resulting in CO_2 adsorption performances that closely mirror those of the untreated material. Besides, preliminary substitution with NH_4^+ prior Li-exchange, has also minimal impact on the ultimate amount of Li in the framework. NH_4-3_Li-3 and NH4-6_Li-3 exhibit CO_2 adsorption behaviors akin to the equally Li-exchanged sample (i.e. Li-3), suggesting that NH_4^+ cations do not substantially affect the subsequent Li^+ incorporation.

2. Optimizing Li content for enhanced adsorption
- Li-content correlation - Increasing the Li-exchange degree from Li-3 to Li-9 leads to a substantial and progressive enhancement of the CO_2 adsorption process (in terms of all the evaluated CO_2 adsorption parameters). The positive correlation between Li content and adsorption performances underscores the potential for carefully optimizing Li-exchange cycles to significantly boost CO_2 capture efficiency.

3. Adsorption isotherms
- Model fitting quality - The Freundlich model proves effective in describing non-ideal multilayer adsorption on synthesized tuff samples. Its consistent good fit to experimental data, as indicated by high coefficients of determination (R^2) and low HYBRID error function values, affirms its suitability.

4. CO_2/N_2 selectivity
- CO_2 is captured in significantly greater quantities than N_2 on Li-9, with selectivity factors varying from 187 in a 2 %/98 % CO_2/N_2 mixture to 40 in a mixture containing 20 %/80 % CO_2/N_2 mixture. These selectivity levels are notably higher than those observed for traditional sorbents like zeolites, activated carbons, and MOFs.

5. Multi-cyclic stability
- Regardless of the specific cation-exchange type applied, the adsorption capacities of all synthesized samples remain unchanged over 10 consecutive adsorption/desorption cycles, aligning with the typical multi-cyclic stability observed in zeolitic materials.

In summary, this research underscores the intricate relationship between cation-exchange processes, particularly with Li and Na, and the resulting CO_2 adsorption behavior in natural tuff. Derived from construction and demolition waste, this material shows promise as an affordable and sustainable CO_2 adsorbent, offering insights that can contribute to optimizing materials and processes for enhanced carbon capture efficiency in the context of climate change mitigation.

CRediT authorship contribution statement

F. Raganati: Conceptualization, Data curation, Writing – original draft, Writing – review & editing, Investigation, Methodology. **F. Miccio:** Conceptualization, Writing – review & editing, Investigation, Methodology. **G. Iervolino:** Investigation, Methodology. **E. Papa:** Investigation. **P. Ammendola:** Conceptualization, Data curation, Writing – original draft, Writing – review & editing, Investigation, Methodology.

Declaration of competing interest

The authors declare that they have no known competing financial interests or personal relationships that could have appeared to influence the work reported in this paper.

Acknowledgement

The authors acknowledge Mr. Cortese (SEM imaging), Mr. Stanzione (ICP-MS analyses) and Mr. Mazzocchi (XRD analysis).

References

[1] P. Ammendola, R. Chirone, G. Ruoppolo, G. Russo, Production of hydrogen from thermo-catalytic decomposition of methane in a fluidized bed reactor, Chem. Eng. J. 154 (2009) 287–294, https://doi.org/10.1016/j.cej.2009.03.048.
[2] D.Y.C. Leung, G. Caramanna, M.M. Maroto-Valer, An overview of current status of carbon dioxide capture and storage technologies, Renew. Sustain. Energy Rev. 39 (2014) 426–443, https://doi.org/10.1016/j.rser.2014.07.093.
[3] A. Samanta, A. Zhao, G.K.H. Shimizu, P. Sarkar, R. Gupta, Post-combustion CO2 capture using solid sorbents: a review, Ind. Eng. Chem. Res. 51 (2012) 1438–1463, https://doi.org/10.1021/ie200686q.
[4] M. Karl, R.F. Wright, T.F. Berglen, B. Denby, Worst case scenario study to assess the environmental impact of amine emissions from a CO2 capture plant, Int. J. Greenhouse Gas Control 5 (2011) 439–447, https://doi.org/10.1016/j.ijggc.2010.11.001.
[5] M.G. Plaza, S. García, F. Rubiera, J.J. Pis, C. Pevida, Post-combustion CO2 capture with a commercial activated carbon: Comparison of different regeneration

strategies, Chem. Eng. J. 163 (2010) 41–47, https://doi.org/10.1016/j.cej.2010.07.030.
[6] F. Raganati, R. Chirone, P. Ammendola, CO 2 capture by temperature swing adsorption: working capacity as affected by temperature and CO 2 Partial pressure, Ind. Eng. Chem. Res. 59 (2020) 3593–3605, https://doi.org/10.1021/acs.iecr.9b04901.
[7] F. Raganati, P. Ammendola, Sound-assisted fluidization for temperature swing adsorption and calcium looping: a review, Materials 14 (2021) 672, https://doi.org/10.3390/ma14030672.
[8] F. Raganati, F. Miccio, P. Ammendola, Adsorption of Carbon dioxide for post-combustion capture: a review, Energy Fuel 35 (2021) 12845–12868, https://doi.org/10.1021/acs.energyfuels.1c01618.
[9] M. Alfe, P. Ammendola, V. Gargiulo, F. Raganati, R. Chirone, Magnetite loaded carbon fine particles as low-cost CO2 adsorbent in a sound assisted fluidized bed, Proc. Combust. Inst. 35 (2015) 2801–2809, https://doi.org/10.1016/j.proci.2014.06.037.
[10] P. Ammendola, F. Raganati, R. Chirone, Effect of operating conditions on the CO2 recovery from a fine activated carbon by means of TSA in a fluidized bed assisted by acoustic fields, Fuel Process. Technol. 134 (2015) 494–501, https://doi.org/10.1016/j.fuproc.2015.03.010.
[11] F. Raganati, P. Ammendola, R. Chirone, On improving the CO2 recovery efficiency of a conventional TSA process in a sound assisted fluidized bed by separating heating and purging, Sep. Purif. Technol. 167 (2016) 24–31, https://doi.org/10.1016/j.seppur.2016.05.001.
[12] F. Raganati, P. Ammendola, R. Chirone, Effect of acoustic field on CO2 desorption in a fluidized bed of fine activated carbon, Particuology 23 (2015) 8–15, https://doi.org/10.1016/j.partic.2015.02.001.
[13] F. Raganati, P. Ammendola, R. Chirone, Role of acoustic fields in promoting the gas-solid contact in a fluidized bed of fine Particles, Kona Powder Part. J. 32 (2015) 23–40, https://doi.org/10.14356/kona.2015006.
[14] V. Gargiulo, M. Alfè, P. Ammendola, F. Raganati, R. Chirone, CO2 sorption on surface-modified carbonaceous support: probing the influence of the carbon black microporosity and surface polarity, Appl. Surf. Sci. 360 (2016) 329–337, https://doi.org/10.1016/j.apsusc.2015.11.026.
[15] M. Hemmat, A. Rahbar-Kelishami, M.H. Vakili, Preparation of carbon molecular sieves and its impregnation with co and ni for CO2/N2 separation, Int. J. Environ. Sci. Technol. 15 (2018) 2213–2228, https://doi.org/10.1007/s13762-017-1526-5.
[16] F. Raganati, P. Ammendola, R. Chirone, CO2 capture by adsorption on fine activated carbon in a sound assisted fluidized bed, Chem. Eng. Trans. 43 (2015) 1033–1038, https://doi.org/10.3303/CET1543173.
[17] F. Raganati, P. Ammendola, R. Chirone, CO2 adsorption on fine activated carbon in a sound assisted fluidized bed: effect of sound intensity and frequency, CO2 partial pressure and fluidization velocity, Appl. Energy 113 (2014) 1269–1282, https://doi.org/10.1016/j.apenergy.2013.08.073.
[18] F. Raganati, P. Ammendola, R. Chirone, CO2 capture performances of fine solid sorbents in a sound-assisted fluidized bed, Powder Technol. 268 (2014) 347–356, https://doi.org/10.1016/j.powtec.2014.08.062.
[19] R. Girimonte, B. Formisani, F. Testa, Adsorption of CO2 on a confined fluidized bed of pelletized 13X zeolite, Powder Technol. 311 (2017) 9–17, https://doi.org/10.1016/j.powtec.2017.01.033.
[20] S.C. Lee, Y.M. Kwon, C.Y. Ryu, H.J. Chae, D. Ragupathy, S.Y. Jung, J.B. Lee, C. K. Ryu, J.C. Kim, Development of new alumina-modified sorbents for CO2 sorption and regeneration at temperatures below 200°C, Fuel (2010) 2–7, https://doi.org/10.1016/j.fuel.2010.11.006.
[21] K.B. Lee, M.G. Beaver, H.S. Caram, S. Sircar, Reversible Chemisorbents for Carbon dioxide and their potential applications, Ind. Eng. Chem. Res. 47 (2008) 8048–8062, https://doi.org/10.1021/ie800795y.
[22] M. Minelli, E. Papa, V. Medri, F. Miccio, P. Benito, F. Doghieri, E. Landi, Characterization of novel geopolymer – zeolite composites as solid adsorbents for CO2 capture, Chem. Eng. J. 341 (2018) 505–515, https://doi.org/10.1016/j.cej.2018.02.050.
[23] M. Minelli, V. Medri, E. Papa, F. Miccio, E. Landi, F. Doghieri, Geopolymers as solid adsorbent for CO2 capture, Chem. Eng. Sci. 148 (2016) 267–274, https://doi.org/10.1016/j.ces.2016.04.013.
[24] J. Bai, J. Huang, Q. Yu, M. Demir, E. Akgul, B.N. Altay, X. Hu, L. Wang, Fabrication of coconut shell-derived porous carbons for CO2 adsorption application, Front. Chem. Sci. Eng. 17 (2023) 1122–1130, https://doi.org/10.1007/S11705-022-2292-6/METRICS.
[25] J. Bai, J. Huang, Q. Yu, M. Demir, M. Kilic, B.N. Altay, X. Hu, L. Wang, N-doped porous carbon derived from macadamia nut shell for CO2 adsorption, Fuel Process. Technol. 249 (2023) 107854, https://doi.org/10.1016/j.fuproc.2023.107854.
[26] J. Bai, J. Huang, Q. Jiang, W. Jiang, M. Demir, M. Kilic, B.N. Altay, L. Wang, X. Hu, Synthesis and characterization of polyphenylene sulfide resin-derived S-doped porous carbons for efficient CO2 capture, Colloids Surf. A Physicochem. Eng. Asp. 674 (2023) 131916, https://doi.org/10.1016/j.colsurfa.2023.131916.
[27] J. Bai, J. Shao, Q. Yu, M. Demir, B. Nazli Altay, T. Muhammad Ali, Y. Jiang, L. Wang, X. Hu, Sulfur-doped porous carbon adsorbent: a promising solution for effective and selective CO2 capture, Chem. Eng. J. 479 (2024) 147667, https://doi.org/10.1016/j.cej.2023.147667.
[28] Y. Sang, Y. Cao, L. Wang, W. Yan, T. Chen, J. Huang, Y.N. Liu, N-rich porous organic polymers based on schiff base reaction for CO2 capture and mercury(II) adsorption, J. Colloid Interface Sci. 587 (2021) 121–130, https://doi.org/10.1016/J.JCIS.2020.12.002.
[29] M.G. Plaza, C. Pevida, J.J. Pis, F. Rubiera, Evaluation of the cyclic capacity of low-cost carbon adsorbents for post-combustion CO2 capture, Energy Procedia 4 (2011) 1228–1234, https://doi.org/10.1016/j.egypro.2011.01.178.
[30] M. Sevilla, J.B. Parra, A.B. Fuertes, Assessment of the role of micropore size and N-doping in CO2 capture by porous carbons, ACS Appl. Mater. Interfaces 5 (2013) 6360–6368, https://doi.org/10.1021/am401423b.
[31] S. Qi, Y. Yu, Z. Yang, X. Liu, X. Lu, X. Liu, L. Sun, Active sites modulation with <scp>Runge–Gross</scp> theorem: <scp> CO $_2$ </scp> capture by porphyrinic metal–organic frameworks at excited states, AIChE J 69 (2023) e17994.
[32] R.V. Siriwardane, M.-S. Shen, E.P. Fisher, J.A. Poston, Adsorption of CO2 on Molecular sieves and activated Carbon, Energy Fuel 15 (2001) 279–284, https://doi.org/10.1021/ef000241s.
[33] N. Gargiulo, K. Shibata, A. Peluso, P. Aprea, T. Valente, G. Pezzotti, T. Shiono, D. Caputo, Reinventing rice husk ash: derived NaX zeolite as a high-performing CO2 adsorbent, Int. J. Environ. Sci. Technol. 15 (2018) 1543–1550, https://doi.org/10.1007/s13762-017-1534-5.
[34] M. Ackley, R. Rege, H. Saxena, Application of natural zeolites in the purification and separation of gases, Microporous Mesoporous Mater. 61 (2003) 25–42, https://doi.org/10.1016/S1387-1811(03)00353-6.
[35] P. Ammendola, F. Raganati, R. Chirone, F. Miccio, Preliminary assessment of tuff as CO2 sorbent, Energy Procedia 114 (2017) 46–52, https://doi.org/10.1016/j.egypro.2017.03.1145.
[36] C. Colella, Applications of Natural Zeolites, in: Handbook of Porous Solids, Wiley-VCH Verlag GmbH, Weinheim, Germany, 2008: pp. 1156–1189. doi: 10.1002/9783527618286.ch18i.
[37] P. Misaelides, Application of natural zeolites in environmental remediation: a short review, Microporous Mesoporous Mater. 144 (2011) 15–18, https://doi.org/10.1016/j.micromeso.2011.03.024.
[38] S. Pallewatta, M. Weerasooriyagedara, S. Bordoloi, A.K. Sarmah, M. Vithanage, Reprocessed construction and demolition waste as an adsorbent: an appraisal, Sci. Total Environ. 882 (2023) 163340, https://doi.org/10.1016/j.scitotenv.2023.163340.
[39] B. S, A. O. D, N. C.W.W, Feasibility of construction demolition waste for unexplored geotechnical and geo-environmental applications- a review, Constr Build Mater 356 (2022) 129230. doi: 10.1016/j.conbuildmat.2022.129230.
[40] V. Paolini, F. Petracchini, E. Guerriero, A. Bencini, S. Drigo, Biogas cleaning and upgrading with natural zeolites from tuffs, Environ. Technol. 37 (2016) 1418–1427, https://doi.org/10.1080/09593330.2015.1118557.
[41] A. Alonso-Vicario, J.R. Ochoa-Gómez, S. Gil-Río, O. Gómez-Jiménez-Aberasturi, C. A. Ramírez-López, J. Torrecilla-Soria, A. Domínguez, Purification and upgrading of biogas by pressure swing adsorption on synthetic and natural zeolites, Microporous Mesoporous Mater. 134 (2010) 100–107, https://doi.org/10.1016/j.micromeso.2010.05.014.
[42] P. Ammendola, F. Raganati, R. Chirone, F. Miccio, Thermodynamic and kinetic Characterization of yellow tuff for CO 2 adsorption, Chem. Eng. Trans. 74 (2019) 1207–1212, https://doi.org/10.3303/CET1974202.
[43] P. Ammendola, F. Raganati, R. Chirone, F. Miccio, Fixed bed adsorption as affected by thermodynamics and kinetics: yellow tuff for CO2 capture, Powder Technol. 373 (2020) 446–458, https://doi.org/10.1016/j.powtec.2020.06.075.
[44] S. Kumar, R. Srivastava, J. Koh, Utilization of zeolites as CO2 capturing agents: advances and future perspectives, J. CO2 Util. 41 (2020) 101251, https://doi.org/10.1016/j.jcou.2020.101251.
[45] K.S. Walton, M.B. Abney, M. Douglas LeVan, CO2 adsorption in Y and X zeolites modified by alkali metal cation exchange, Microporous Mesoporous Mater. 91 (2006) 78–84, https://doi.org/10.1016/j.micromeso.2005.11.023.
[46] D. Barthomeuf, Framework induced basicity in zeolites, Microporous Mesoporous Mater. 66 (2003) 1–14, https://doi.org/10.1016/j.micromeso.2003.08.006.
[47] M. Cavallo, M. Dosa, N.G. Porcaro, F. Bonino, M. Piumetti, V. Crocellà, Shaped natural and synthetic zeolites for CO2 capture in a wide temperature range, J. CO2 Util. 67 (2023) 102335, https://doi.org/10.1016/j.jcou.2022.102335.
[48] H.-T. Vu, M. Goepel, R. Gläser, Improving the hydrothermal stability of zeolite Y by la 3+ cation exchange as a catalyst for the aqueous-phase hydrogenation of levulinic acid, RSC Adv. 11 (2021) 5568–5579, https://doi.org/10.1039/D0RA08907A.
[49] M.V. Gil, N. Álvarez-Gutiérrez, M. Martínez, F. Rubiera, C. Pevida, A. Morán, Carbon adsorbents for CO2 capture from bio-hydrogen and biogas streams: breakthrough adsorption study, Chem. Eng. J. 269 (2015) 148–158, https://doi.org/10.1016/j.cej.2015.01.100.
[50] F. Raganati, M. Alfe, V. Gargiulo, R. Chirone, P. Ammendola, Kinetic study and breakthrough analysis of the hybrid physical/chemical CO2 adsorption/desorption behavior of a magnetite-based sorbent, Chem. Eng. J. 372 (2019) 526–535, https://doi.org/10.1016/j.cej.2019.04.165.
[51] P. Ammendola, F. Raganati, R. Chirone, CO2 adsorption on a fine activated carbon in a sound assisted fluidized bed: thermodynamics and kinetics, Chem. Eng. J. 322 (2017) 302–313, https://doi.org/10.1016/j.cej.2017.04.037.
[52] M.F. Freundlich, Over the adsorption in solution, J. Phys. Chem. 57 (1906) 355–471.
[53] D. Tiwari, C. Goel, H. Bhunia, P.K. Bajpai, Dynamic CO2 capture by carbon adsorbents: kinetics, isotherm and thermodynamic studies, Sep. Purif. Technol. 181 (2017) 107–122, https://doi.org/10.1016/j.seppur.2017.03.014.
[54] M. Saleh Shafeeyan, W. Mohd Ashri Wan Daud, A. Shamiri, N. Aghamohammadi, Adsorption equilibrium of carbon dioxide on ammonia-modified activated carbon, Chem. Eng. Res. Des. 104 (2015) 42–52, https://doi.org/10.1016/j.cherd.2015.07.018.
[55] J. Sreńscek-Nazzal, U. Narkiewicz, A.W. Morawski, R. Wróbel, A. Gęsikiewicz-Puchalska, B. Michalkiewicz, Modification of Commercial activated Carbons for CO 2 adsorption, Acta Phys. Pol. A 129 (2016) 394–401, https://doi.org/10.12693/APhysPolA.129.394.

[56] D. Iruretagoyena Ferrer, Supported Layered Double Hydroxides as CO2 Adsorbents for Sorption-enhanced H2 Production, Springer International Publishing, Cham, 2016. doi: 10.1007/978-3-319-41276-4.
[57] J. a. Mason, K. Sumida, Z.R. Herm, R. Krishna, Jeffrey.R. Long, Evaluating metal–organic frameworks for post-combustion carbon dioxide capture via temperature swing adsorption, Energy Environ. Sci. 4 (2011) 3030–3040. doi: 10.1039/c1ee01720a.
[58] S.-C. Hsu, C. Lu, F. Su, W. Zeng, W. Chen, Thermodynamics and regeneration studies of CO2 adsorption on multiwalled carbon nanotubes, Chem. Eng. Sci. 65 (2010) 1354–1361, https://doi.org/10.1016/j.ces.2009.10.005.
[59] Y. Yang, C. Sitprasert, T.E. Rufford, L. Ge, P. Shukla, S. Wang, V. Rudolph, Z. Zhu, An experimental and simulation study of binary adsorption in metal–organic frameworks, Sep. Purif. Technol. 146 (2015) 136–142, https://doi.org/10.1016/j.seppur.2015.03.041.
[60] M.M.J. Treacy, J.B. Higgins, Collection of simulated XRD powder patterns for zeolites, Elsevier, 2001.
[61] S. Özen, M.C. Göncüoğlu, B. Liguori, B. de Gennaro, P. Cappelletti, G.D. Gatta, F. Iucolano, C. Colella, A comprehensive evaluation of sedimentary zeolites from Turkey as pozzolanic addition of cement- and lime-based binders, Constr. Build. Mater. 105 (2016) 46–61, https://doi.org/10.1016/j.conbuildmat.2015.12.055.
[62] A. Alshameri, A. Ibrahim, A.M. Assabri, X. Lei, H. Wang, C. Yan, The investigation into the ammonium removal performance of yemeni natural zeolite: modification, ion exchange mechanism, and thermodynamics, Powder Technol. 258 (2014) 20–31, https://doi.org/10.1016/j.powtec.2014.02.063.
[63] A. Gęsikiewicz-Puchalska, M. Zgrzebnicki, B. Michalkiewicz, A. Kałamaga, U. Narkiewicz, A.W. Morawski, R. Wrobel, Changes in porous Parameters of the ion exchanged X zeolite and their effect on CO2 adsorption, Molecules 26 (2021) 7520, https://doi.org/10.3390/molecules26247520.
[64] D.M. Ruthven, Principles of adsorption and adsorption processes, John Wiley & Sons, 1984.
[65] N. Álvarez-Gutiérrez, M.V. Gil, F. Rubiera, C. Pevida, Kinetics of CO2 adsorption on cherry stone-based carbons in CO2/CH4 separations, Chem. Eng. J. 307 (2017) 249–257, https://doi.org/10.1016/j.cej.2016.08.077.
[66] F. Raganati, M. Alfe, V. Gargiulo, R. Chirone, P. Ammendola, Isotherms and thermodynamics of CO2 adsorption on a novel carbon-magnetite composite sorbent, Chem. Eng. Res. Des. 134 (2018) 540–552, https://doi.org/10.1016/j.cherd.2018.04.037.
[67] B. Guo, L. Chang, K. Xie, Adsorption of Carbon dioxide on activated Carbon, J. Nat. Gas Chem. 15 (2006) 223–229, https://doi.org/10.1016/S1003-9953(06)60030-3.
[68] B. Selen, A. Glayan, A.E. Aksoylu, CO2 adsorption behavior and kinetics on chemically modified activated carbons, Turk. J. Chem. 40 (2016) 576–587. doi: 10.3906/kim-1507-95.
[69] X. Zhou, H. Yi, X. Tang, H. Deng, H. Liu, Thermodynamics for the adsorption of SO2, NO and CO2 from flue gas on activated carbon fiber, Chem. Eng. J. 200–202 (2012) 399–404, https://doi.org/10.1016/j.cej.2012.06.013.
[70] A. Golchoobi, H. Pahlavanzadeh, Molecular simulation, experiments and modelling of single adsorption capacity of 4A molecular sieve for CO 2 –CH 4 separation, Sep. Sci. Technol. 51 (2016) 2318–2325, https://doi.org/10.1080/01496395.2016.1206571.
[71] J.-S. Lee, J.-H. Kim, J.-T. Kim, J.-K. Suh, J.-M. Lee, C.-H. Lee, Adsorption equilibria of CO 2 on zeolite 13X and zeolite X/Activated Carbon composite, J. Chem. Eng. Data 47 (2002) 1237–1242, https://doi.org/10.1021/je020050e.
[72] X. Xu, X. Zhao, L. Sun, X. Liu, Adsorption separation of carbon dioxide, methane, and nitrogen on hβ and na-exchanged β-zeolite, J. Nat. Gas Chem. 17 (2008) 391–396, https://doi.org/10.1016/S1003-9953(09)60015-3.
[73] M.A. Hernandez, A. Pestryakov, R. Portillo, M.A. Salgado, F. Rojas, E. Rubio, S. Ruiz, V. Petranovskii, CO2 sequestration by natural zeolite for greenhouse effect control, Procedia Chem. 15 (2015) 33–41, https://doi.org/10.1016/j.proche.2015.10.006.
[74] L. Hauchhum, P. Mahanta, Carbon dioxide adsorption on zeolites and activated carbon by pressure swing adsorption in a fixed bed, Int. J. Energy Environ. Eng. 5 (2014) 349–356, https://doi.org/10.1007/s40095-014-0131-3.
[75] R. Sips, On the structure of a catalyst Surface, J. Chem. Phys. 16 (1948) 490–495, https://doi.org/10.1063/1.1746922.
[76] J. Toth, State equations of the solid-gas Interface layers, Acta Chimica Academiae Scientiarum Hungaricae 69 (1971) 311–328.
[77] W. Baek, S. Ha, S. Hong, S. Kim, Y. Kim, Cation exchange of cesium and cation selectivity of natural zeolites: chabazite, stilbite, and heulandite, Microporous Mesoporous Mater. 264 (2018) 159–166, https://doi.org/10.1016/j.micromeso.2018.01.025.
[78] T.D. Pham, M.R. Hudson, C.M. Brown, R.F. Lobo, Molecular basis for the high CO 2 adsorption capacity of chabazite zeolites, ChemSusChem 7 (2014) 3031–3038, https://doi.org/10.1002/cssc.201402555.
[79] A. Heydari-Gorji, A. Sayari, CO2 capture on polyethylenimine-impregnated hydrophobic mesoporous silica: Experimental and kinetic modeling, Chem. Eng. J. 173 (2011) 72–79, https://doi.org/10.1016/j.cej.2011.07.038.
[80] V.K. Singh, E. Anil Kumar, Measurement and analysis of adsorption isotherms of CO2 on activated carbon, Appl. Therm. Eng. 97 (2016) 77–86, https://doi.org/10.1016/j.applthermaleng.2015.10.052.
[81] Y. Belmabkhout, A. Sayari, Effect of pore expansion and amine functionalization of mesoporous silica on CO2 adsorption over a wide range of conditions, Adsorption 15 (2009) 318–328, https://doi.org/10.1007/s10450-009-9185-6.
[82] A. Koide, T. Kihara, Intermolecular forces for D2, N2, O2, F2 and CO2, Chem. Phys. (1974), https://doi.org/10.1016/0301-0104(74)80004-2.
[83] S. Himeno, T. Tomita, K. Suzuki, S. Yoshida, Characterization and selectivity for methane and carbon dioxide adsorption on the all-silica DD3R zeolite, Microporous Mesoporous Mater. 98 (2007) 62–69, https://doi.org/10.1016/j.micromeso.2006.05.018.
[84] P. Ning, F. Li, H. Yi, X. Tang, J. Peng, Y. Li, D. He, H. Deng, Adsorption equilibrium of methane and carbon dioxide on microwave-activated carbon, Sep. Purif. Technol. 98 (2012) 321–326, https://doi.org/10.1016/j.seppur.2012.07.001.
[85] J. Zhang, R. Singh, P.A. Webley, Alkali and alkaline-earth cation exchanged chabazite zeolites for adsorption based CO2 capture, Microporous Mesoporous Mater. 111 (2008) 478–487, https://doi.org/10.1016/j.micromeso.2007.08.022.
[86] S.-T. Yang, J. Kim, W.-S. Ahn, CO2 adsorption over ion-exchanged zeolite beta with alkali and alkaline earth metal ions, Microporous Mesoporous Mater. 135 (2010) 90–94, https://doi.org/10.1016/j.micromeso.2010.06.015.
[87] M.M. Zagho, M.K. Hassan, M. Khraisheh, M.A.A. Al-Maadeed, S. Nazarenko, A review on recent advances in CO2 separation using zeolite and zeolite-like materials as adsorbents and fillers in mixed matrix membranes (MMMs), Chem. Eng. J. Adv. 6 (2021) 100091, https://doi.org/10.1016/j.ceja.2021.100091.
[88] J.K. Bower, D. Barpaga, S. Prodinger, R. Krishna, H.T. Schaef, B.P. McGrail, M. A. Derewinski, R.K. Motkuri, Dynamic adsorption of CO 2 /N 2 on cation-exchanged chabazite SSZ-13: a breakthrough analysis, ACS Appl. Mater. Interfaces 10 (2018) 14287–14291, https://doi.org/10.1021/acsami.8b03848.